Computational stabilization of a non-heme iron enzyme enables efficient evolution of new function

Authors

Brianne R. King, Kiera H. Sumida, Jessica L. Caruso, David Baker, and Jesse G. Zalatan*

Corresponding Author

Jesse G. Zalatan − Department of Chemistry, University of Washington, Seattle, Washington 98195, United States; Email: zalatan@uw.edu

Authors

Brianne R. King − Department of Chemistry, University of Washington, Seattle, Washington 98195, United States

Kiera H. Sumida − Department of Chemistry and Institute for Protein Design, University of Washington, Seattle, Washington 98195, United States

Jessica L. Caruso − Department of Chemistry, University of Washington, Seattle, Washington 98195, United States

David Baker − Institute for Protein Design, Department of Biochemistry, and Howard Hughes Medical Institute, University of Washington, Seattle, Washington 98195, United States

Abstract

Directed evolution has emerged as a powerful tool for engineering new biocatalysts. However, introducing new catalytic residues can be destabilizing, and it is generally beneficial to start with a stable enzyme parent. Here we show that the deep learning-based tool ProteinMPNN can be used to redesign Fe(II)/αKG superfamily enzymes for greater stability, solubility, and expression while retaining both native activity and industrially-relevant non-native functions. For the Fe(II)/αKG enzyme tP4H, we performed site-saturation mutagenesis with both the wild-type and stabilized design variant and screened for activity increases in a non-native C-H hydroxylation reaction. We observed substantially larger increases in non-native activity for variants obtained from the stabilized scaffold compared to those from the wild-type enzyme. ProteinMPNN is user-friendly and widely-accessible, and straightforward structural criteria were sufficient to obtain stabilized, catalytically-functional variants of the Fe(II)/αKG enzymes tP4H and GriE. Our work suggests that stabilization by computational sequence redesign could be routinely implemented as a first step in directed evolution campaigns for novel biocatalysts.

Introduction

Directed evolution is a powerful method to generate enzymes for new chemical transformations.[1,2] However, catalytic functional groups often have destabilizing effects on protein structure, and altering active site groups for new reactions can lead to unstable, non-functional proteins.[3–11] Initiating a directed evolution campaign from a stabilized variant can be an effective way to overcome this problem.[12,13] Typically, a starting point for directed evolution is obtained by screening a library of candidate enzymes for a desired promiscuous activity. If a thermostable homolog with similar catalytic properties is identified, it can then be used as a starting point for evolution of the desired function.[14,15] Alternatively, there are a variety of strategies to produce stable variants using directed evolution,[16,17] ancestral reconstruction,[14] protein recombination,[18,19] or computational engineering.[20–22] These methods are often time- and resource-intensive, highlighting the need for simple and accessible alternatives.

An important class of enzymes where stabilization would be useful is the non-heme iron(II) α-ketoglutarate-dependent oxygenase (Fe(II)/αKG) superfamily. These enzymes have emerged as a rich source of potential new biocatalysts. Fe(II)/αKG enzymes can perform asymmetric C-H oxyfunctionalization reactions on small molecule substrates, which could allow expedient and sustainable diversification of simple building blocks to a range of complex polyfunctional compounds.[23–26] The advantages offered by this enzyme family include a high degree of chemical flexibility in the iron-containing active site due to multiple open coordination sites, the utilization of benign molecular oxygen as an oxidant, and use of the inexpensive and readily available co-factor αKG. However, Fe(II)/αKGs can be relatively unstable,[27,28] which may limit their practical applications in organic synthesis.

57 The recent use of an Fe(II)/αKG in an industrial-scale drug biosynthesis pathway highlights
58 both the potential advantages and drawbacks of this family for biocatalysis. An engineered
59 Fe(II)/αKG was used to catalyze an enantioselective C-H hydroxylation to produce a key
60 intermediate for the anti-cancer drug belzutifan.[28] The reaction could be performed on kilogram-
61 scale and bypassed five steps of the pre-existing chemical synthesis route. Notably, this effort
62 required an extensive, large-scale directed evolution campaign. Furthermore, early rounds of
63 screening yielded stabilizing mutations before significant improvements in turnover could be
64 obtained in later rounds. These findings highlight the potential utility of Fe(II)/αKG for practical,
65 industrial-scale green chemistry but also the importance of enzyme stability in the evolution of
66 new function.

67 Recent applications of deep learning to protein design have provided new and relatively
68 straightforward methods to stabilize protein scaffolds,[22,29,30] and there is broad interest in applying
69 these approaches to directed evolution.[31] Here we demonstrate that the deep learning-based tool
70 ProteinMPNN[29,30] enables more efficient optimization of a synthetically-relevant, non-native C-H
71 hydroxylation reaction in an Fe(II)/αKG family member. A critical step was restricting the
72 redesign from modifying active site and adjacent residues, which would otherwise be readily
73 mutated to stabilize the enzyme. With a stabilized starting point for site-saturation mutagenesis,
74 we observed substantially larger increases in non-native activity compared to the same mutations
75 in the wild-type parent enzyme. We suggest that this designed stabilization approach should be
76 routinely used in future directed evolution campaigns with the Fe(II)/αKG superfamily and will
77 likely be effective in a broad range of other enzyme families.
78

Results and Discussion

Fe(II)/αKGs with promiscuous activity for C-H hydroxylation of free carboxylate substrates

Within the Fe(II)/αKG enzyme superfamily, free amino acid hydroxylases are attractive candidates for engineering new reactions.[23–26] Because Fe(II)/αKG amino acid hydroxylases already have catalytic machinery to interact with amine and carboxylate functional groups in amino acids, we hypothesized that they might have promiscuous activity for substrates containing only an amine or only a carboxylate. These molecules are important feedstocks for early-stage oxyfunctionalization reactions in multi-step syntheses. Selectivity for these reactions has been historically difficult to achieve with traditional transition metal catalysis, and a biocatalytic process could offer improved regio- and stereoselectivity.[32,33]

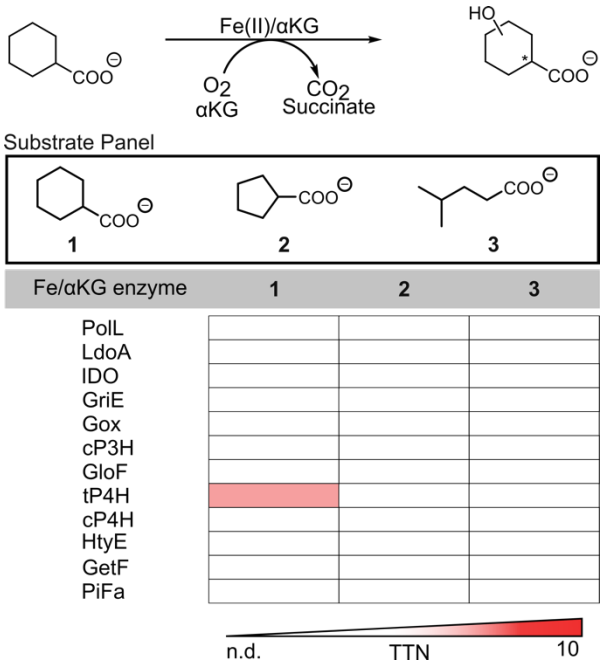

Figure 1. Initial whole-cell reaction screen data with a panel of Fe(II)/αKG amino acid hydroxylases and free acid substrate analogues. Reactions were performed in whole cell from 50 mL expression cultures where whole cell volume was 1/20th the expression volume. Reactions were carried out in MOPS (pH 7.0, 50 mM) with 20 mM substrate, 60 mM αKG (as disodium salt), 1 mM ferrous ammonium sulfate, and 1 mM L-ascorbic acid.

95 We initially screened a panel of 12 Fe(II)/αKG amino acid hydroxylases for the ability to
96 hydroxylate free carboxylates (Figure 1). We chose a set of candidate carboxylate substrates (**1-3**)
97 that are structurally analogous to the native amino acid substrates L-pipecolic acid, L-proline, and
98 L-leucine. We used whole-cell biocatalysis and liquid chromatography-mass spectrometry (LC-
99 MS) to detect products. We confirmed that the native amino acid reaction products are detectable
100 with all 12 members of the enzyme panel (Table S6). We then screened for promiscuous activity
101 with carboxylates, and observed that one enzyme, tP4H,[34] has detectable activity with substrate **1**
102 (Figure 1). The total turnover number (TTN) with this substrate was ~5 after 24 hr incubation with
103 10 μM enzyme, ~130-fold lower than the TTN for the corresponding native amino acid substrate.
104 The reaction of tP4H with substrate **1** gives the *trans* product with a *d.r.* of 4:1 (Figure S4). tP4H
105 produces exclusively *trans* product with its native substrate L-pipecolic acid,[34] suggesting that the
106 free carboxylate substrate **1** and the native substrate are positioned similarly in the enzyme active
107 site with respect to the iron center. To confirm that tP4H and not a contaminating enzyme was
108 responsible for the observed non-native activity, we mutated active site residues that are involved
109 in Fe(II), substrate, or αKG binding. Because tP4H does not have an experimental structure, we
110 identified these active site residues using an Alphafold2[35] model (Figure S9) and comparisons to
111 structures of the highly homologous Fe(II)/αKG enzyme GriE.[36,37] In all cases, active site
112 mutations produced activity decreases for the non-native substrate **1** (Figure 2). We also observed
113 increased product yield with increasing wild-type tP4H concentration (Figure 2). Together these
114 results confirm that tP4H is responsible for the non-native reaction.

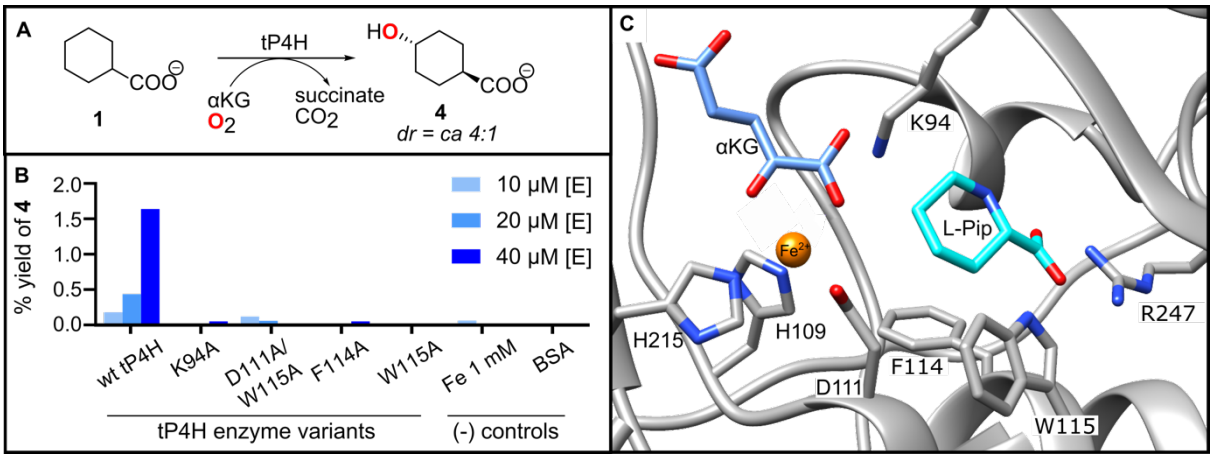

Figure 2. Validation of tP4H activity with free acid **1.** (A) Reaction of tP4H with substrate **1** to form *trans*-4-hydroxycyclohexane carboxylic acid **4**. (B) Yield of **4** after reaction of **1** with tP4H variants, as well as negative control reaction with Fe(II) and bovine serum albumin (BSA). The Fe 1 mM control was run in the absence of added enzyme. Purified enzyme concentration was varied between 10-40 μM with 20 mM **1**, 40 mM αKG, 1 mM ferrous ammonium sulfate, and 1 mM L-ascorbic acid in MES buffer (50 mM, pH 6.8). Reactions were carried out for 24 hours at 25 °C and quantified with analytical LC-MS. (C) Structural model of the tP4H showing key active site residues. Fe(II), αKG, and L-Pipecolic acid were modeled in Chimera.[38]

Stabilization of tP4H with ProteinMPNN

To improve tP4H activity towards substrate **1**, we began a directed evolution campaign but quickly encountered limitations due to poor enzyme stability. First, we found that tP4H variants were difficult to express and purify due to enzyme insolubility. Additionally, we found that the parent wild-type tP4H enzyme loses activity with time (Figure 3). These observations are consistent with prior reports on tP4H behavior.[34] It is possible for enzyme stability to improve during directed evolution, whether by selecting more stable variants during each round or by chance. For example, the evolved Fe(II)/αKG PsEFE had slight stability improvements compared to wild-type, despite the researchers not selecting for improved stability.[39] In another case, the Fe(II)/αKG UbP4H was successfully screened for improved stability after initial screening rounds destabilized the enzyme.[27] However, the benefits of starting with a highly stable enzyme for directed evolution are well-established.[12–14] A stabilized protein scaffold could potentially increase

137 the population of active, properly-folded protein or provide access to other mutants that otherwise
138 do not fold.

139 We used the deep learning-based tool ProteinMPNN[29,30] to generate stabilized variants of
140 tP4H through sequence design. We first used ProteinMPNN to redesign the entire tP4H sequence.
141 Unsurprisingly, we found that the predicted sequences eliminated key active site residues, which
142 is likely to disrupt enzymatic activity (Figure S10). This behavior is consistent with the well-
143 established propensity for catalytic active site residues to be destabilizing.[3–10] To preserve catalytic
144 function, we fixed the active site residues in all subsequent design efforts. We defined the active
145 site as any residues that contact the amino acid substrate, Fe(II), or the αKG cofactor, based on our
146 Alphafold2 model (Figure S9) and comparisons to the structure of the closely-related enzyme GriE
147 bound to L-leucine.[37] Because other residues throughout the protein could also be important, we
148 also tested four additional strategies using either sequence conservation or distance metrics. To
149 identify important conserved residues, we constructed a multiple sequence alignment (MSA) and
150 selected tP4H residues conserved in at least 35%, 70%, or 95% of sequences (Methods and Table
151 S4). Alternatively, we fixed any residues with side chains within a 10 Å sphere from the substrate
152 binding pocket. Using these five starting points (fix active site only, active site + 35%/70%/95%
153 conservation, active site + 10 Å sphere), we generated 48 ProteinMPNN sequences per method
154 and selected 4 each (20 total) for activity screens. Selection was based on calculated top-ranked
155 Cα-RMSD values matched to the input tP4H structure. We obtained only one variant that had any
156 detectable activity, with catalytic efficiency ~35-fold lower than wild-type tP4H (Figure S11). This
157 variant was designed from the sequence where >35% conserved residues are fixed, which
158 constrains more residues than the >70% or >95% cutoffs. This result suggests that even weakly
159 conserved residues may need to be fixed to maintain activity. Further analysis of the variant with

160 detectable activity revealed a ~3.5-fold increase in the K_M for the αKG cofactor (Figure S11). We
161 identified two residues in proximity to αKG, L228 and V230, that were mutated in the redesigned
162 sequence. These sequence changes may have contributed to improved stability at the expense of
163 cofactor binding and positioning, leading to the decrease in activity. Notably, L228 and V230 were
164 fixed in the designs generated from fixed active site + 10 Å sphere, but none of these designs had
165 detectable activity. Taken together, these findings suggest that additional criteria will be needed to
166 identify critical functional residues that should be fixed prior to sequence redesign.

167 To generate stabilized variants that maintain catalytic activity, we performed another set
168 of ProteinMPNN sequence redesigns with three new strategies to fix important residues. In each
169 case, we fixed the active site as defined above plus residues L228 and V230. For the first approach,
170 we fixed all residues at tP4H positions conserved in 35% of the MSA. We chose this cutoff because
171 it was the only one from our initial set that produced a stabilized variant with any detectable
172 activity, and we expected that fixing L228 or V230 could further improve these designs. For the
173 second and third approaches, we identified highly conserved positions regardless of whether the
174 wild-type tP4H residue is the most highly conserved amino acid. These strategies were based on
175 previous work suggesting that more stringent constraints are necessary to maintain activity in
176 ProteinMPNN redesign.[30] Every tP4H amino acid position was ranked based on the %
177 conservation of the most frequent amino acid present in the MSA, and the top 50% or 70% were
178 fixed as the wild-type tP4H residue. Together with fixed active site residues, these criteria resulted
179 in 148/272 (54%) or 198/272 (73%) fixed residues across the entire 272 amino acid protein. Using
180 these three strategies, we selected 32 designs each of 48 generated for a total of 96 sequences
181 (Supplementary spreadsheet – ProteinMPNN sequences_metrics). Of these designs, 69 expressed
182 detectable quantities of protein by SDS-PAGE and 11 had detectable activity above background

183 for the native substrate. For the active enzymes we proceeded to measure thermostability and
184 kinetic parameters for the native L-pipecolic acid substrate and the promiscuous carboxylate
185 substrate **1**. The variant with the highest k_{cat} for L-pipecolic acid was R2_11 (Table S7), with a k_{cat}
186 of 0.16 s^{-1} compared to 0.17 s^{-1} for wild-type. R2_11 was designed from the method where the top
187 70% ranked conserved residues were fixed, and had 44 designed mutations compared to the wild-
188 type sequence (Figure 3). R2_11 has modestly slower (~3-fold) non-native carboxylate
189 hydroxylase activity compared to wild-type tP4H and exhibits a 20 °C increase in thermostability
190 by temperature-dependent circular dichroism (CD) spectroscopy (Figure 3). When activity is
191 measured as a function of time, R2_11 maintains activity over a timescale of days, which is a
192 substantial improvement compared to wild-type tP4H (Figure 3).
193

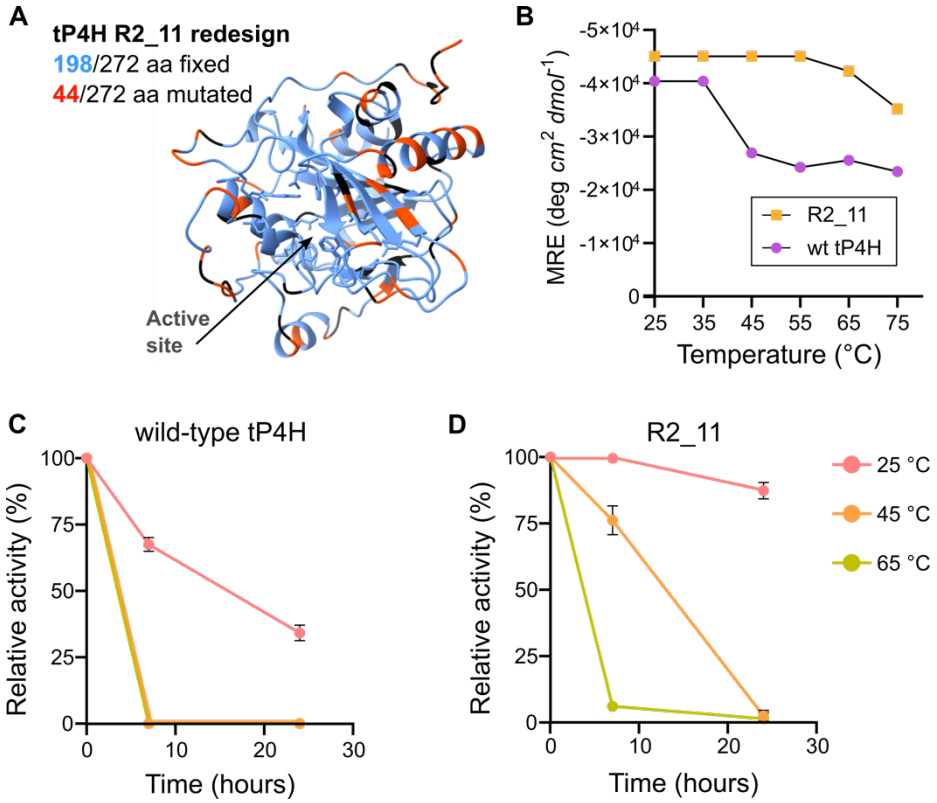

194

195 Figure 3. Stability and activity of wild-type tP4H and ProteinMPNN design R2_11. (A) tP4H structure
196 (Alphafold2 model, Figure S9) color-coded to show sites fixed in the design process (blue, Supplementary

spreadsheet – ProteinMPNN sequences_metrics) and sites mutated in the ProteinMPNN R2_11 redesign (orange-red). Sites colored black were neither fixed nor redesigned in the R2_11 variant. Side chains for first shell active site residues (Table S4) are shown in blue. (B) Temperature-dependent CD spectroscopy of wild-type tP4H and R2_11. (C) Activity-stability analysis of wild-type tP4H. (D) Activity-stability analysis of R2_11. Relative activity was determined using PBP assay described in Supplementary Information.

Stabilization of GriE with ProteinMPNN

After successfully identifying sequence constraints for ProteinMPNN-mediated stabilization of tP4H while maintaining catalytic function, we evaluated whether the same approach would be effective with a second Fe(II)/αKG enzyme, GriE. This enzyme could benefit from stabilization because, although it expresses well and is soluble, it loses activity at room temperature over 24 hours (Figure S12). As with tP4H, we fixed the top 70% ranked conserved residues along with catalytic residues identified from the GriE crystal structure (Supplementary spreadsheet – ProteinMPNN sequences_metrics).[37] We generated 32 redesigned sequences and found that 29 were expressed as soluble enzyme, and 27 showed activity with the GriE native substrate L-leucine. The top design based on stability and kinetic parameters, GM_A9, showed a catalytic efficiency (k_{cat}/K_M) 4-fold lower than wild-type GriE (Figure S12 & S13). One design, GM_A11, had a 2-fold faster initial rate with L-leucine compared to GM_A9 but this design was unstable by temperature-dependent CD and thus was not chosen for further analysis. For GM_A9, the decrease in catalytic efficiency arises from a lower k_{cat} of 0.38 s^{-1} compared to our measured k_{cat} of 2.1 s^{-1} for wild-type GriE. A decrease in catalytic efficiency is not surprising given that increased stability could reduce conformational flexibility and negatively impact catalytic function.[4,6,7]

We next screened the stabilized GriE redesign GM_A9 for substrate promiscuity. Previously, wild-type GriE has been shown to accept substrates with increased substrate chain lengths but has weaker activity towards substrates with substitution at C3.[40] We chose two previously identified non-native substrates to test: L-norleucine and L-allo-isoleucine. L-

225 norleucine was chosen as a representative substrate with increased chain length compared to L-
226 leucine. L-allo-isoleucine was chosen because it has a methyl group substitution at C3. We
227 observed detectable activity with L-norleucine but not for L-allo-isoleucine (Table S8). Similar to
228 wild-type GriE, the GM_A9 variant maintained a preference for the extended chain L-norleucine
229 substrate over the C3-substituted L-allo-isoleucine substrate. The GM-A9 reactions with L-leucine
230 and L-norleucine were 11- and 4-fold slower than wild-type GriE reactions, respectively (Table
231 S8). These results suggest that our ProteinMPNN protocol can be readily applied to other
232 Fe(II)/αKG enzymes to stabilize proteins while maintaining synthetically-relevant catalytic
233 function that can be a foothold for further optimization by directed evolution.

234 *Directed evolution of wild-type tP4H for carboxylate C-H hydroxylation activity*

235 We next sought to improve the non-native carboxylate hydroxylase activity through
236 directed evolution. We prioritized tP4H because carboxylate hydroxylase activity was detectable
237 in both the wild-type and ProteinMPNN-stabilized variant, which allows for direct comparisons.
238 We conducted three rounds of directed evolution for both enzymes by varying first- and second-
239 shell substrate binding residues identified in the active site from our Alphafold2 structural model.
240 We defined the first shell as any residues that contact the amino acid substrate, based on
241 comparisons to the structure of ligand-bound GriE.[37] We defined the second shell as any residues
242 that make contacts with first shell residues. We used the 22c-trick method for single site-saturation
243 mutagenesis at each target position.[41]

244 We first performed directed evolution with wild-type tP4H. For the first screening round,
245 we chose three tP4H active site residues based on their potential role in substrate specificity: H58,
246 F114, and L174. Based on our tP4H structural model (Figure S9B), H58 likely contacts the amine
247 of native amino acid substrates and is presumably not needed or detrimental for carboxylate

248 substrates that lack an amine. F114 likely provides a substrate hydrophobic contact, and L174 is
249 part of a loop that could affect substrate binding. We screened whole cell biocatalysis reactions in
250 96 well plates for improved TTN and 80% *trans* selectivity in reactions with substrate **1**. Based on
251 production of hydroxylated product **4**, the top 5% of mutants were chosen for validation with
252 purified enzymes. We obtained several variants with modest activity improvements, and the best
253 performer was mutant H58L with a TTN of 7 (Figure 4A). In a second round starting from H58L,
254 we rescreened mutants at F114 and L174 and screened an additional 14 first and second shell
255 residues (Table S1). We identified the improved variant H58L/W170Q with a TTN of 15. In a
256 third round starting from H58L/W170Q, we screened 9 residues that showed activity increases in
257 previous rounds and identified the improved variant H58L/W170Q/E118K with a TTN of 31
258 (Figure 4A & Table S1). Overall, after three rounds of directed evolution for improved carboxylate
259 hydroxylase activity with wild-type tP4H we obtained a 6-fold improvement in TTN and
260 maintained >80% selectivity for the *trans* reaction product (Figure S4).
261

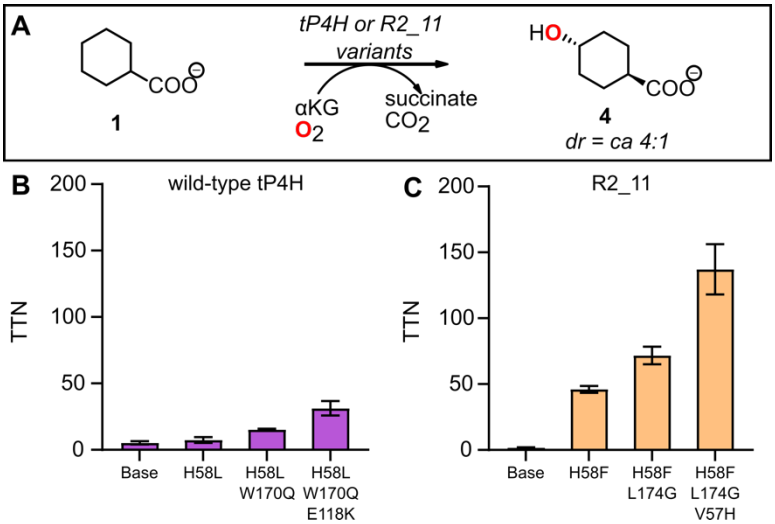

262
263
264 Figure 4. (A) Reaction scheme for C-H hydroxylation of substrate **1** with tP4H, R2_11, and associated
265 variants. (B) Directed evolution of wild-type tP4H. (C) Directed evolution of stabilized variant R2_11.
266 Reactions were carried out for 24 hr at 25 °C using purified enzyme (10-20 μM) in MES buffer (50 mM, pH
267 6.8), with 20 mM cyclohexane carboxylic acid **1**, 40 mM αKG, 1 mM ferrous ammonium sulfate, and 1 mM

ascorbic acid. Concentration of **4** in quenched reaction samples was quantified by analytical LC-MS analysis.

Directed evolution of ProteinMPNN redesign R2_11 for carboxylate C-H hydroxylation activity.

To optimize carboxylate hydroxylase activity in ProteinMPNN-stabilized tP4H, we conducted directed evolution using a similar strategy to our approach with wild-type tP4H, with minor modifications. In the first round of site saturation mutagenesis, we started with a larger pool of 19 first- and second-shell residues including the three sites from prior round one (H58, F114, and L174) and the 16 additional sites from prior round 2 (Table S1). As before, we screened whole cell biocatalysis reactions for improved TTN and >80% *trans* selectivity with carboxylic acid substrate **1**. The top hit was H58F, which is the same position but a different mutant than the previous round one winner, H58L. R2_11_H58F displayed a 27-fold increase in TTN relative to the parent R2_11 (Figure 4B). This effect is substantially bigger than the <2-fold improvement obtained with H58L relative to wild-type tP4H. Notably, the 27-fold increase in a single round from stabilized R2_11 was already larger than the total 6-fold improvement from three rounds of directed evolution from wild-type tP4H. Given the strong performance of the H58F mutant, we also evaluated its effect in the wild-type tP4H background and observed a small, <2-fold increase in TTN, similar to the effect of H58L on wild-type tP4H (Figure S14). Thus, the strong, 27-fold improvement with the H58F mutant depends on the context of the stabilized R2_11 backbone.

In a second round of screening from R2_11_H58F, we selected the 18 residues that were screened in prior round two from wild-type tP4H (Table S1). We retained this large pool of residues to ensure a direct comparison to the tP4H directed evolution workflow. This round identified improved variant L174G. R2_11_H58F/L174G has a TTN of 72. This TTN is a 1.6-fold improvement from parent R2_11_H58F and outstrips any variant obtained from the wild-type tP4H backbone (Figure 4B). In a third round of screening from R2_11_H58F/L174G, we selected

294 9 residues that were screened in prior round 3 from wild-type tP4H (Table S1). This round
295 identified the improved variant V57H with a TTN of 138, a 1.7-fold improvement from the
296 previous round.

297 Overall, the ProteinMPNN-stabilized tP4H directed evolution campaign produced an 80-
298 fold improvement in TTN from the base R2_11 redesign, compared to a modest 6-fold
299 improvement in the wild-type tP4H evolutionary trajectory. Although the R2_11 parent starts ~3-
300 fold slower than wild-type tP4H, the much larger improvement over three rounds of directed
301 evolution produced an R2_11 triple mutant with a 4.5-fold higher TTN than the triple mutant
302 obtained from wild-type tP4H (Figure 4).

303 In addition to a more efficient directed evolution trajectory, the R2_11 triple mutant
304 maintains high stability relative to the wild-type tP4H and associated variants from directed
305 evolution (Figure 5A, Figure S15). Higher stability allows reactions to be run more efficiently,
306 both at higher temperatures and for less time. For example, after 6 hours at 35 °C, the R2_11 triple
307 mutant reaches a mean TTN of 142 for the non-native reaction with carboxylate **1** to form product
308 **4** with 4:1 selectivity for the *trans* reaction product (Figure 5B). The TTN after 6 hours at 35 °C
309 is comparable to the TTN after 24 hours at 25 °C. In contrast, the tP4H triple mutant shows a slight
310 decrease in TTN at 35 °C, likely due to enzyme instability at higher temperatures (Figure 5B). The
311 stability profile of the R2_11 triple mutant suggests that this enzyme will be more robust towards
312 further engineering compared to the tP4H triple mutant. Future engineering efforts with the R2_11
313 mutant could include improvements to key reaction metrics like turnover, selectivity, and
314 increased substrate scope.

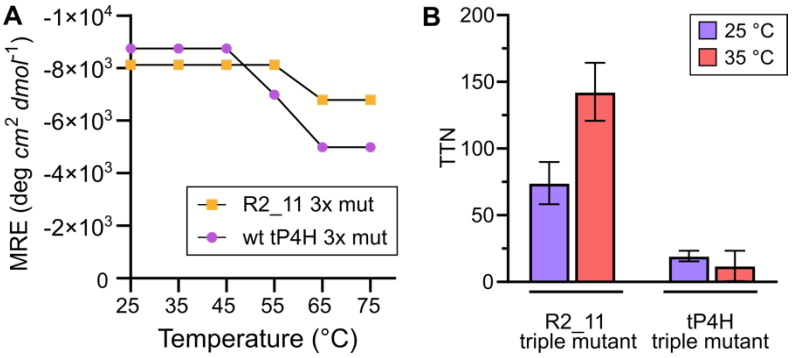

Figure 5 A) Temperature dependent CD of the R2_11 and tP4H triple mutants. B) TTN for formation of **4** (*d.r.* 4:1, Figure S4) with the R2_11 and tP4H triple mutants at two different temperatures. Reactions were carried out for 6 hrs. at 25 °C and 35 °C using purified enzyme (15 μM) in MES buffer (50 mM, pH 6.8), with 20 mM cyclohexane carboxylic acid **1**, 40 mM αKG, 1 mM ferrous ammonium sulfate, and 1 mM ascorbic acid.

Conclusions

Directed evolution is a powerful tool to engineer enzymes for new-to-nature reactions. However, many enzyme starting points for evolution may lack the stability required to reach user-defined optimum fitness after multiple rounds of mutagenesis. Here we show that the deep learning-based tool ProteinMPNN can be used to stabilize the Fe(II)/αKG enzyme superfamily members tP4H and GriE with straightforward sequence constraints to maintain catalytic activity. Consistent with previous results using ProteinMPNN,[30] the top tP4H design was identified by using the most conservative of our chosen methods for fixing residues during sequence redesign. Applying the same method to the related enzyme GriE readily produced stabilized variants with catalytic activity.

Wild-type and redesigned tP4H both exhibit novel reactivity towards remote C-H hydroxylation of a free carboxylic acid substrate. We directly compared evolutionary trajectories of wild-type tP4H with the stabilized variant R2_11 and demonstrated superior performance of the stabilized redesign variant. Future work will determine if this design method is generalizable to optimize directed evolution for other enzymes and enzyme families. User-friendly deep learning-

337 based tools like ProteinMPNN and MutCompute are rapidly emerging,[22,29,30] and our work
338 suggests that these tools should be routinely incorporated into enzyme engineering workflows to
339 efficiently optimize catalytic fitness for new biocatalysts.[31]
340

341 **Supplementary Information**

342 Materials, experimental and analytical methods, compound characterization data (Figure S4-S7),
343 and enzyme characterization data (Figure S3, Figure S8, Figure S11-S15 and Tables S6-S8) (PDF).
344 Accession numbers for all Fe(II)/αKG enzymes used in this work, full nucleotide and amino acid
345 sequences for all reported wild-type and enzyme variants, oligonucleotide sequences for cloning
346 and for all ProteinMPNN designs, ProteinMPNN design screen criteria results (XLSX).

347

Acknowledgements

We thank Dr. Wolfgang Hüttel at the University of Freiburg and Hans Renata at Rice University for the donation of the wild-type tP4H and GriE expression vectors, respectively, and for their advice on tP4H and GriE reactions in various formats. We also thank Jonathan Zhang and Susanna Vazquez Torres for their early contributions to Fe(II)/αKG reaction screening, and Dr. Martin Sadilek in University of Washington Mass Spectrometry Facility for his continued support and helpful advice in analytical method development. This work was supported by U.S. National Institutes of Health grants T32 GM008268 (B.R.K., J.L.C.) and R35 GM124773 (J.G.Z.), and by the Open Philanthropy Project Improving Protein Design Fund (K.H.S., D.B.).

Competing Interests

The authors declare that they have no competing interests.

References

(1) Renata, H.; Wang, Z. J.; Arnold, F. H. Expanding the Enzyme Universe: Accessing Non-Natural Reactions by Mechanism-Guided Directed Evolution. *Angew. Chem. Int. Ed.* **2015**, *54* (11), 3351–3367. https://doi.org/10.1002/anie.201409470.

(2) Zeymer, C.; Hilvert, D. Directed Evolution of Protein Catalysts. *Annu. Rev. Biochem.* **2018**, *87* (1), 1–27. https://doi.org/10.1146/annurev-biochem-062917-012034.

(3) Meiering, E. M.; Serrano, L.; Fersht, A. R. Effect of Active Site Residues in Barnase on Activity and Stability. *J. Mol. Biol.* **1992**, *225* (3), 585–589. https://doi.org/10.1016/0022-2836(92)90387-y.

(4) Shoichet, B. K.; Baase, W. A.; Kuroki, R.; Matthews, B. W. A Relationship between Protein Stability and Protein Function. *Proc. Natl. Acad. Sci.* **1995**, *92* (2), 452–456. https://doi.org/10.1073/pnas.92.2.452.

(5) Giver, L.; Gershenson, A.; Freskgard, P.-O.; Arnold, F. H. Directed Evolution of a Thermostable Esterase. *Proc. Natl. Acad. Sci.* **1998**, *95* (22), 12809–12813. https://doi.org/10.1073/pnas.95.22.12809.

(6) Beadle, B. M.; Shoichet, B. K. Structural Bases of Stability–Function Tradeoffs in Enzymes. *J. Mol. Biol.* **2002**, *321* (2), 285–296. https://doi.org/10.1016/s0022-2836(02)00599-5.

(7) Nagatani, R. A.; Gonzalez, A.; Shoichet, B. K.; Brinen, L. S.; Babbitt, P. C. Stability for Function Trade-Offs in the Enolase Superfamily "Catalytic Module". *Biochemistry* **2007**, *46* (23), 6688–6695. https://doi.org/10.1021/bi700507d.

(8) Tokuriki, N.; Stricher, F.; Serrano, L.; Tawfik, D. S. How Protein Stability and New Functions Trade Off. *PLoS Comput. Biol.* **2008**, *4* (2), e1000002. https://doi.org/10.1371/journal.pcbi.1000002.

(9) Tokuriki, N.; Jackson, C. J.; Afriat-Jurnou, L.; Wyganowski, K. T.; Tang, R.; Tawfik, D. S. Diminishing Returns and Tradeoffs Constrain the Laboratory Optimization of an Enzyme. *Nat. Commun.* **2012**, *3* (1), 1257. https://doi.org/10.1038/ncomms2246.

(10) Goldsmith, M.; Tawfik, D. S. Enzyme Engineering: Reaching the Maximal Catalytic Efficiency Peak. *Curr. Opin. Struct. Biol.* **2017**, *47*, 140–150. https://doi.org/10.1016/j.sbi.2017.09.002.

(11) Tsuboyama, K.; Dauparas, J.; Chen, J.; Laine, E.; Behbahani, Y. M.; Weinstein, J. J.; Mangan, N. M.; Ovchinnikov, S.; Rocklin, G. J. Mega-Scale Experimental Analysis of Protein Folding Stability in Biology and Design. *Nature* **2023**, *620* (7973), 434–444. https://doi.org/10.1038/s41586-023-06328-6.

395 (12) Bloom, J. D.; Labthavikul, S. T.; Otey, C. R.; Arnold, F. H. Protein Stability Promotes
396 Evolvability. *Proc. Natl. Acad. Sci.* **2006**, *103* (15), 5869–5874.
397 https://doi.org/10.1073/pnas.0510098103.

398 (13) Gumulya, Y.; Baek, J.-M.; Wun, S.-J.; Thomson, R. E. S.; Harris, K. L.; Hunter, D. J. B.;
399 Behrendorff, J. B. Y. H.; Kulig, J.; Zheng, S.; Wu, X.; Wu, B.; Stok, J. E.; Voss, J. J. D.; Schenk,
400 G.; Jurva, U.; Andersson, S.; Isin, E. M.; Bodén, M.; Guddat, L.; Gillam, E. M. J. Engineering
401 Highly Functional Thermostable Proteins Using Ancestral Sequence Reconstruction. *Nat. Catal.*
402 **2018**, *1* (11), 878–888. https://doi.org/10.1038/s41929-018-0159-5.

403 (14) Trudeau, D. L.; Tawfik, D. S. Protein Engineers Turned Evolutionists—the Quest for the
404 Optimal Starting Point. *Curr. Opin. Biotechnol.* **2019**, *60*, 46–52.
405 https://doi.org/10.1016/j.copbio.2018.12.002.

406 (15) Besenmatter, W.; Kast, P.; Hilvert, D. Relative Tolerance of Mesostable and Thermostable
407 Protein Homologs to Extensive Mutation. *Proteins: Struct., Funct., Bioinform.* **2007**, *66* (2),
408 500–506. https://doi.org/10.1002/prot.21227.

409 (16) Socha, R. D.; Tokuriki, N. Modulating Protein Stability – Directed Evolution Strategies for
410 Improved Protein Function. *FEBS J.* **2013**, *280* (22), 5582–5595.
411 https://doi.org/10.1111/febs.12354.

412 (17) Stimple, S. D.; Smith, M. D.; Tessier, P. M. Directed Evolution Methods for Overcoming
413 Trade-offs between Protein Activity and Stability. *AIChE J.* **2020**, *66* (3).
414 https://doi.org/10.1002/aic.16814.

415 (18) Li, Y.; Drummond, D. A.; Sawayama, A. M.; Snow, C. D.; Bloom, J. D.; Arnold, F. H. A
416 Diverse Family of Thermostable Cytochrome P450s Created by Recombination of Stabilizing
417 Fragments. *Nat. Biotechnol.* **2007**, *25* (9), 1051–1056. https://doi.org/10.1038/nbt1333.

418 (19) Heinzelman, P.; Snow, C. D.; Wu, I.; Nguyen, C.; Villalobos, A.; Govindarajan, S.;
419 Minshull, J.; Arnold, F. H. A Family of Thermostable Fungal Cellulases Created by Structure-
420 Guided Recombination. *Proc. Natl. Acad. Sci.* **2009**, *106* (14), 5610–5615.
421 https://doi.org/10.1073/pnas.0901417106.

422 (20) Goldenzweig, A.; Goldsmith, M.; Hill, S. E.; Gertman, O.; Laurino, P.; Ashani, Y.; Dym,
423 O.; Unger, T.; Albeck, S.; Prilusky, J.; Lieberman, R. L.; Aharoni, A.; Silman, I.; Sussman, J. L.;
424 Tawfik, D. S.; Fleishman, S. J. Automated Structure- and Sequence-Based Design of Proteins for
425 High Bacterial Expression and Stability. *Mol. Cell* **2016**, *63* (2), 337–346.
426 https://doi.org/10.1016/j.molcel.2016.06.012.

427 (21) Musil, M.; Konegger, H.; Hon, J.; Bednar, D.; Damborsky, J. Computational Design of
428 Stable and Soluble Biocatalysts. *ACS Catal.* **2019**, *9* (2), 1033–1054.
429 https://doi.org/10.1021/acscatal.8b03613.

(22) Lu, H.; Diaz, D. J.; Czarnecki, N. J.; Zhu, C.; Kim, W.; Shroff, R.; Acosta, D. J.; Alexander, B. R.; Cole, H. O.; Zhang, Y.; Lynd, N. A.; Ellington, A. D.; Alper, H. S. Machine Learning-Aided Engineering of Hydrolases for PET Depolymerization. *Nature* **2021**, *604* (7907), 662–667. https://doi.org/10.1038/s41586-022-04599-z.

(23) Islam, M. S.; Leissing, T. M.; Chowdhury, R.; Hopkinson, R. J.; Schofield, C. J. 2-Oxoglutarate-Dependent Oxygenases. *Annu. Rev. Biochem.* **2018**, *87*, 585–620. https://doi.org/10.1146/annurev-biochem-061516-044724.

(24) Herr, C. Q.; Hausinger, R. P. Amazing Diversity in Biochemical Roles of Fe(II)/2-Oxoglutarate Oxygenases. *Trends Biochem Sci* **2018**, *43* (7), 517–532. https://doi.org/10.1016/j.tibs.2018.04.002.

(25) Papadopoulou, A.; Meyer, F.; Buller, R. M. Engineering Fe(II)/α-Ketoglutarate-Dependent Halogenases and Desaturases. *Biochemistry* **2022**. https://doi.org/10.1021/acs.biochem.2c00115.

(26) Zwick, C. R.; Renata, H. Harnessing the Biocatalytic Potential of Iron- and α-Ketoglutarate-Dependent Dioxygenases in Natural Product Total Synthesis. *Nat. Prod. Rep.* **2020**, *37* (8), 1065–1079. https://doi.org/10.1039/c9np00075e.

(27) Liu, C.; Zhao, J.; Liu, J.; Guo, X.; Rao, D.; Liu, H.; Zheng, P.; Sun, J.; Ma, Y. Simultaneously Improving the Activity and Thermostability of a New Proline 4-Hydroxylase by Loop Grafting and Site-Directed Mutagenesis. *Appl. Microbiol. Biotechnol.* **2019**, *103* (1), 265–277. https://doi.org/10.1007/s00253-018-9410-x.

(28) Cheung-Lee, W. L.; Kolev, J. N.; McIntosh, J. A.; Gil, A. A.; Pan, W.; Xiao, L.; Velásquez, J. E.; Gangam, R.; Winston, M. S.; Li, S.; Abe, K.; Alwedi, E.; Dance, Z. E. X.; Fan, H.; Hiraga, K.; Kim, J.; Kosjek, B.; Le, D. N.; Marzijarani, N. S.; Mattern, K.; McMullen, J. P.; Narsimhan, K.; Vikram, A.; Wang, W.; Yan, J.; Yang, R.; Zhang, V.; Zhong, W.; DiRocco, D. A.; Morris, W. J.; Murphy, G. S.; Maloney, K. M. Engineering Hydroxylase Activity, Selectivity, and Stability for a Scalable Concise Synthesis of a Key Intermediate to Belzutifan. *Angew. Chem. Int. Ed.* **2024**, *63* (13), e202316133. https://doi.org/10.1002/anie.202316133.

(29) Dauparas, J.; Anishchenko, I.; Bennett, N.; Bai, H.; Ragotte, R. J.; Milles, L. F.; Wicky, B. I. M.; Courbet, A.; Haas, R. J. de; Bethel, N.; Leung, P. J. Y.; Huddy, T. F.; Pellock, S.; Tischer, D.; Chan, F.; Koepnick, B.; Nguyen, H.; Kang, A.; Sankaran, B.; Bera, A. K.; King, N. P.; Baker, D. Robust Deep Learning–Based Protein Sequence Design Using ProteinMPNN. *Science* **2022**, *378* (6615), 49–56. https://doi.org/10.1126/science.add2187.

(30) Sumida, K. H.; Núñez-Franco, R.; Kalvet, I.; Pellock, S. J.; Wicky, B. I. M.; Milles, L. F.; Dauparas, J.; Wang, J.; Kipnis, Y.; Jameson, N.; Kang, A.; Cruz, J. D. L.; Sankaran, B.; Bera, A. K.; Jiménez-Osés, G.; Baker, D. Improving Protein Expression, Stability, and Function with ProteinMPNN. *J. Am. Chem. Soc.* **2024**. https://doi.org/10.1021/jacs.3c10941.

(31) Yang, J.; Li, F.-Z.; Arnold, F. H. Opportunities and Challenges for Machine Learning-Assisted Enzyme Engineering. *ACS Cent. Sci.* **2024**, *10* (2), 226–241. https://doi.org/10.1021/acscentsci.3c01275.

(32) Roduner, E.; Kaim, W.; Sarkar, B.; Urlacher, V. B.; Pleiss, J.; Gläser, R.; Einicke, W.; Sprenger, G. A.; Beifuß, U.; Klemm, E.; Liebner, C.; Hieronymus, H.; Hsu, S.; Plietker, B.; Laschat, S. Selective Catalytic Oxidation of C-H Bonds with Molecular Oxygen. *ChemCatChem* **2013**, *5* (1), 82–112. https://doi.org/10.1002/cctc.201200266.

(33) He, C.; Whitehurst, W. G.; Gaunt, M. J. Palladium-Catalyzed C(Sp3)–H Bond Functionalization of Aliphatic Amines. *Chem* **2019**, *5* (5), 1031–1058. https://doi.org/10.1016/j.chempr.2018.12.017.

(34) Klein, C.; Hüttel, W. A Simple Procedure for Selective Hydroxylation of L-Proline and L-Pipecolic Acid with Recombinantly Expressed Proline Hydroxylases. *Adv. Synth. Catal.* **2011**, *353* (8), 1375–1383. https://doi.org/10.1002/adsc.201000863.

(35) Mirdita, M.; Schütze, K.; Moriwaki, Y.; Heo, L.; Ovchinnikov, S.; Steinegger, M. ColabFold: Making Protein Folding Accessible to All. *Nat. Methods* **2022**, *19* (6), 679–682. https://doi.org/10.1038/s41592-022-01488-1.

(36) Hu, X.; Huang, X.; Liu, J.; Zheng, P.; Gong, W.; Yang, L. Structures of L-Proline Trans-Hydroxylase Reveal the Catalytic Specificity and Provide Deeper Insight into AKG-Dependent Hydroxylation. *Acta Crystallogr. Sect. D* **2023**, *79* (Pt 4), 318–325. https://doi.org/10.1107/s2059798323001936.

(37) Lukat, P.; Katsuyama, Y.; Wenzel, S.; Binz, T.; König, C.; Blankenfeldt, W.; Brönstrup, M.; Müller, R. Biosynthesis of Methyl-Proline Containing Griselimycins, Natural Products with Anti-Tuberculosis Activity. *Chem Sci* **2017**, *8* (11), 7521–7527. https://doi.org/10.1039/c7sc02622f.

(38) Pettersen, E. F.; Goddard, T. D.; Huang, C. C.; Couch, G. S.; Greenblatt, D. M.; Meng, E. C.; Ferrin, T. E. UCSF Chimera—A Visualization System for Exploratory Research and Analysis. *J. Comput. Chem.* **2004**, *25* (13), 1605–1612. https://doi.org/10.1002/jcc.20084.

(39) Goldberg, N. W.; Knight, A. M.; Zhang, R. K.; Arnold, F. H. Nitrene Transfer Catalyzed by a Non-Heme Iron Enzyme and Enhanced by Non-Native Small-Molecule Ligands. *J. Am. Chem. Soc.* **2019**, *141* (50), 19585–19588. https://doi.org/10.1021/jacs.9b11608.

(40) Zwick, C. R.; Renata, H. Remote C–H Hydroxylation by an α-Ketoglutarate-Dependent Dioxygenase Enables Efficient Chemoenzymatic Synthesis of Manzacidin C and Proline Analogs. *J. Am. Chem. Soc.* **2018**, *140* (3), 1165–1169. https://doi.org/10.1021/jacs.7b12918.

(41) Kille, S.; Acevedo-Rocha, C. G.; Parra, L. P.; Zhang, Z.-G.; Opperman, D. J.; Reetz, M. T.; Acevedo, J. P. Reducing Codon Redundancy and Screening Effort of Combinatorial Protein

500 Libraries Created by Saturation Mutagenesis. *ACS Synth. Biol.* **2013**, *2* (2), 83–92.
501 https://doi.org/10.1021/sb300037w.

502

503